ACS APPLIED MATERIALS & INTERFACES

Research Article

www.acsami.org

Enhanced Rate Performance of Mesoporous Co_3O_4 Nanosheet Supercapacitor Electrodes by Hydrous RuO_2 Nanoparticle Decoration

R. B. Rakhi, Wei Chen, M. N. Hedhili, Dongkyu Cha, and H. N. Alshareef*

Material Science and Engineering, King Abdullah University of Science and Technology (KAUST), Thuwal 23955-6900, Saudi Arabia

Supporting Information

ABSTRACT: Mesoporous cobalt oxide (Co_3O_4) nanosheet electrode arrays are directly grown over flexible carbon paper substrates using an economical and scalable two-step process for supercapacitor applications. The interconnected nanosheet arrays form a three-dimensional network with exceptional supercapacitor performance in standard two electrode configuration. Dramatic improvement in the rate capacity of the Co_3O_4 nanosheets is achieved by electrodeposition of nanocrystalline, hydrous RuO_2 nanoparticles dispersed on the Co_3O_4 nanosheets. An optimum RuO_2 electrodeposition time is found to result in the best supercapacitor performance, where the controlled morphology of the electrode provides a balance between good conductivity and efficient electrolyte access to the RuO_2 nanoparticles. An excellent specific capacitance of 905 F/g at 1 A/g is obtained, and a nearly constant rate performance of 78% is achieved at current density ranging from 1 to 40 A/g. The sample could retain more than 96% of its maximum capacitance even after 5000 continuous charge-discharge cycles at a constant high current density of 10 A/g. Thicker RuO_2 coating, while maintaining good conductivity, results in agglomeration, decreasing electrolyte access to active material and hence the capacitive performance.

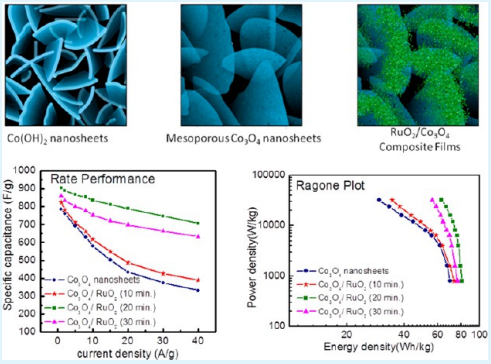

KEYWORDS: *Co_3O_4 nanosheets, supercapacitor, electrodeposition, specific capacitance, rate performance*

1. INTRODUCTION

Supercapacitors, with their higher power densities, fast charge−discharge rates, and excellent cycle stabilities than batteries, and higher energy densities than conventional dielectric capacitors, are devices that promise to cater to the increasing power demands of the 21st century.[1−3] Significant advances in energy density, cycling stability, and rate capability are essential for implementation of supercapacitors in next generation electric vehicles.[3,4] In order to exploit the complete potential of supercapacitors as energy storage devices, further developments in the engineering of electrode materials are required, as the properties of electrode materials like morphology, crystallinity, porosity, capacitive performance, etc., play a key role in determining supercapacitor performance.[3,5,6] It remains specifically challenging to fabricate high-performance supercapacitors with environmentally friendly materials for energy storage.[7,8]

Depending on different energy storage mechanisms, supercapacitors could be classified into two categories, viz. electrochemical double-layer capacitors (EDLCs) and pseudocapacitors. In EDLCs (which are based on high-surface area carbon materials), the capacitance arises from the charge separation at the electrode/electrolyte interface.[9] The capacitance of pseudocapacitors arises mainly from the surface faradaic redox reactions between electrolytes and electrode materials.[1] Apart from this, a certain contribution (5−10%) from the double layer capacitance completely depending on the electrochemically accessible interfacial area between the electrolyte−electrode surfaces, also contributes to the total capacitance.[8,10] Hence, pseudo-capacitors exhibit higher values of capacitance and energy densities as compared to the EDLCs. Transition metal oxides (TMOs) or conducting polymers with several oxidation states for oxidation and reduction are generally used as the electrode materials for pseudocapacitors.[11,12] Among the different TMOs, hydrous ruthenium oxide (RuO_2) has been proven to be an excellent candidate for pseudocapacitor electrode material due to its large specific capacitance (700 F/g), low resistivity, high chemical and thermodynamic stability under electrochemical environment and good reversibility.[13,14] But its commercial application is restricted due to its lack of abundance and high cost.[13] The cost factor can be reduced either by replacing RuO_2 with inexpensive alternative materials or by loading RuO_2 on nanocarbon or other TMOs. Cobalt oxide (Co_3O_4), manganese oxide (MnO_2), nickel oxide (NiO), titanium oxide (TiO_2), zinc oxide (ZnO), tin oxide (SnO_2), etc., can be used as inexpensive alternatives for hydrous RuO_2.[15] Reports are also available on fabrication and performance studies of supercapacitors based on electrodes obtained by loading of RuO_2 in other cheap materials (such as RuO_2/NiO, RuO_2/SnO_2, RuO_2/TiO_2, RuO_2/carbon nanotube, and RuO_2/mesoporous carbon). Loading of RuO_2 in other transition metal oxides can have

Received: December 19, 2013
Accepted: February 28, 2014
Published: February 28, 2014

good capacitive behavior because of incorporation of other transition metal oxides into RuO_2 structure.[16]

With its favorable pseudocapacitive performance, low cost, long-term performance, and good corrosion stability and environmentally friendly nature, Co_3O_4 can be considered as a promising alternative electrode material for high performance pseudocapacitors.[12,17,18] The two major disadvantages with Co_3O_4 systems are lack of reversibility and degradation of capacitance at higher current densities, which can be overcome by incorporation of hydrous RuO_2 nanoparticles.[16,19,20] High-rate charge−discharge and the specific capacitance contribution from RuO_2 can improve the performance of Co_3O_4 /RuO_2 composite based supercapacitor electrode materials.[19,20] A variety of reports are available on the synthesis of Co_3O_4 nanostructures with different morphologies by chemical methods.[21,22] From these reports it has been established that Co_3O_4 nanostructures grown directly over conducting substrates show better supercapacitor performance as compared to commonly used binder-enriched electrodes produced by the slurry coating of Co_3O_4 nanomaterials over conducting substrates, where a large portion of the electroactive surface of electrode materials is blocked from direct contact with the electrolyte. In the case of direct growth, the tedious process of mixing active materials with binders can be avoided as each one of nanostructure will be having its own electrical contact with the conducting substrate, which in turn reduces the internal resistance of the electrode.[18]

Electrochemical deposition is a simple, low cost, and scalable method for the direct growth of Co_3O_4 thin films over conducting substrates. Electrodeposition of Co_3O_4 oxide thin films on copper substrates were reported by Kandalkar et al.[23] and they could achieve a specific capacitance of 235 F/g at a san rate of 20 mV/s. Wu et al. reported the synthesis of porous nanowall Co_3O_4 film Ni foam substrate by scalable electrodeposition technique. The resultant electrode exhibited a specific capacitance of 325 F/g at a current density of 2 A/g and a rate performance of 76% at the current densities ranging from 1 A/g to 10 A/g, in standard 3 electrode configuration.[24] Yuan et al. reported the preparation of porous Co_3O_4 film by a cathodic electrodeposition via liquid crystalline template over Nickel substrate. The resultant electrode exhibited a specific capacitance of 443 F/g in three electrode configuration.[25] In a recent work, Yuan et al. reported a facile, cost-effective and scalable two-step route for the synthesis of well-designed Co_3O_4 nanosheet arrays on Ni foam for high-performance electrochemical capacitors.[26] They could achieve an ultra high specific capacitance of 2735 F/g at a current density of 1 A/g in three electrode configuration. But it has been well established the heightened sensitivity of the three electrode configuration can lead to an overstatement of supercapacitor performance of an electrode material.[27] It has also been reported that substantial errors to the specific capacitance values of electrode materials using nickel foam as current collector.[28] In this particular work by Yuan et al., the capacitance of the sample decreased to 1471 F/g at a current density of 10 A/g with a rate performance of 53% at the current densities ranging from 1 A/g to 10 A/g.[26]

Nature of the electrolyte used also plays a significant role in tuning the electrochemical performance of supercapacitor electrodes. Cobalt oxide electrodes are reported to have good electrochemical performance in alkaline solutions due to their ability to interact with electrolyte ions not only at the surface, but also throughout the bulk.[29] Many reports are available on the wide use of aqueous KOH or NaOH as electrolytes in Co_3O_4 based supercapacitors.[21,22,30−32] In a recent report, Fedorov et al. pointed out that conventional alkaline solutions used for evaluating capacitive performance of electrodeposited cobalt hydroxide/oxides have many disadvantages such as corrosive nature, environmental unfriendliness, besides providing only a small working potential range.[33]They proposed the use of neutral electrolyte solutions such as Na_2SO_4, which are more environmentally friendly and are less corrosive.[33] But the capacitance obtained in the neutral solution was lower than that obtained in alkaline solution.

In this work, we report the direct growth of mesoporous Co_3O_4 nanosheet arrays over flexible carbon paper collectors. Our approach utilizes very small amounts of hydrous RuO_2 nanoparticles to decorate the mesoporous nanosheets of Co_3O_4 resulting in dramatic improvements in the conductivity, supercapacitance, cycle life, and rate capacity of the hybrid RuO_2/Co_3O_4 electrodes.

2. EXPERIMENTAL SECTION

2.1. Electrodeposition of Mesoporous Co_3O_4 Nanosheet Arrays on Carbon Paper Substrate. All reagents in the experiment are of analytical grade, which were used as received without further treatment. Graphitized carbon paper (1 cm × 2 cm) was carefully cleaned by rinsing with deionized water and absolute ethanol and then dried in air. The electrodeposition was performed in a standard three-electrode configuration in a glass cell consisting of the clean carbon paper as working electrode, a platinum wire counter electrode and a saturated calomel reference electrode (SCE) at room temperature of 25 ± 1 °C. The $Co(OH)_2$ was electrodeposited upon carbon paper substrate in a 0.05 M $Co(NO_3)_2{\cdot}6H_2O$ aqueous electrolyte using an CHI 660 D Electrochemical Workstation at a constant potential of −1 V (vs. SCE). After electrodeposition for 30 min, the carbon substrate was carefully rinsed several times with deionized water and absolute ethanol with the assistance of ultrasonication, and finally dried in air. Then, the sample was put in a quartz tube and calcined at 250 °C for 2 h for the conversion of $Co(OH)_2$ nanosheets into mesoporous Co_3O_4 nanosheets. Mass of the Co-based deposit was determined carefully by weighing the sample after calcination.

2.2. Electrodeposition of Nanocrystalline RuO_2 over Co_3O_4 Nanosheet Array. Nanocrystalline RuO_2 particles were electrodeposited over $Co(OH)_2$ nanosheet array (prior to calcination) using the CHI 660D electrochemical workstation from 0.01 M aqueous electrolyte solution of $RuCl_3{\cdot}xH_2O$ which was kept in a water bath at 333 K. Platinum wire and saturated calomel electrode (SCE) were used as a counter and reference electrodes, respectively. The electrodeposition was performed at a constant potential of −1 V (vs. SCE) for three different times, 10, 20, and 30 min. Resultant samples were rinsed several times in deionized water and ethanol, and then dried in air. The samples were then subjected to calcination at 250 °C for 2 h.

2.3. General Characterization of Composites. Samples were characterized by a powder X-ray diffraction system (XRD, Bruker, D8 ADVANCE) equipped with Cu Kα radiation (λ = 0.15406 nm) and X-ray photoelectron spectroscopy (XPS). BET surface area of the samples were determined using surface area and porosimetry system "Micromeritics" (ASAP 2420) at 77 K. Before measurements, the samples were dried at 70 °C for 10 h in a Vacuum oven and then degassed at 200 °C for 12 h until the vacuum was less than 2 μm Hg. The surface morphology and microstructure of the samples were investigated by a scanning electron microscopy (SEM, FEI Helios NanoLab) and transmission electron microscopy (TEM, FEI Titan) and the elemental presence and composition were identified using energy-dispersive X-ray analysis (EDAX).

2.4. Electrochemical Measurement. Electrochemical measurements were carried out in both two- and three-electrode configurations using a model 660D electrochemical workstation (CH Instruments). Assembled coin cells for the two-electrode configuration were

prepared by sandwiching two identical pieces of the samples, pure Co_3O_4 and Co_3O_4/RuO_2 composites prepared by 10, 20, and 30 min deposition of RuO_2 electrodes (each with area containing 1 mg of the total deposit), by a monolayer polypropylene separator (25 μm thick, Celgard 3501), inside a coin cell (CR2032, MTI), with 30 wt % KOH (Sigma Aldrich) as electrolyte. For the measurements in the three-electrode configuration, the individual sample was used as working electrode, Ag/AgCl as reference electrode, Pt wire as counter electrode, and 30 wt % KOH as electrolyte.

Cyclic voltammogram (CV), galvanostatic charge–discharge (CD) and electrochemical impedance spectroscopy (EIS) were performed to evaluate the electrochemical performance of symmetric supercapacitors. The CVs were tested in a voltage window between 0 and 0.8 V at a wide range of scan rates, ranging from 1 mV/s to 100 V/s. The CDs were measured in the same voltage window under a wide range of current densities, from 1 A/g to 40 A/g. EIS measurements were performed both in 3 and 2 electrode configurations. The EIS was performed in the frequency range from 100 kHz to 10 mHz at open circuit voltage by applying a 5 mV signal. All measurements were carried out at room temperature.

Specific capacitance (C_{sp}) of symmetric supercapacitors were calculated from the cyclic voltammogramms and charge-discharge curves according to eq 1 and 2

$$C_{sp} = \frac{2i}{fm} \tag{1}$$

where i is average cathodic current of CV loop and f is the scan rate.

$$C_{sp} = \left(\frac{2i}{m}\right)\left(\frac{dv}{dt}\right)^{-1} \tag{2}$$

where i is the constant current for charge–discharge, (dv/dt) is slope of the discharge curve, and m is the mass of one electrode. In the present study, for specific capacitance calculation electrode mass was taken as 1 mg (mass of the active materials only).

3. RESULTS AND DISCUSSION

Schematic of the synthesis strategy is shown in Figure 1. The preparation process of Co_3O_4 nanosheet arrays mainly involves two steps. In the first step, $Co(OH)_2$ precursors of green color are electrodeposited onto the carbon paper substrate. When the electrical current passes through the electrolyte containing $Co(NO_3)_2$, nitrate ions can be reduced on the cathodic surface to produce hydroxide ions. The generation of OH^- ions at the cathode raises the local pH value, resulting in a uniform precipitation of $Co(OH)_2$ on the surface of the graphitized carbon paper. The chemical reactions involved in this process can be explained as follows:[34,35]

$$NO_3^- + H_2O + 2e^- \Leftrightarrow NO_2^- + 2OH^- \tag{3}$$

$$Co^{2+} + 2OH^- \Leftrightarrow Co(OH)_2 \tag{4}$$

Second step is the calcination process at 250 °C, where, $Co(OH)_2$ is thermally transformed to black Co_3O_4 supported on the carbon paper substrate, which can be explained using the following simple oxidation reaction

$$6Co(OH)_2 + O_2 \Leftrightarrow 2Co_3O_4 + 6H_2O \tag{5}$$

Synthesis of Co_3O_4 /RuO_2 films involves three steps. The first step is the electrodeposition of green color $Co(OH)_2$ precursors on carbon paper. In the second step, hydrated RuO_2 ($RuO_2{\cdot}xH_2O$) is electrodeposited over $Co(OH)_2$ deposit from an aqueous solution of $RuCl_3{\cdot}xH_2O$ according to the method demonstrated by Park et al.[36]

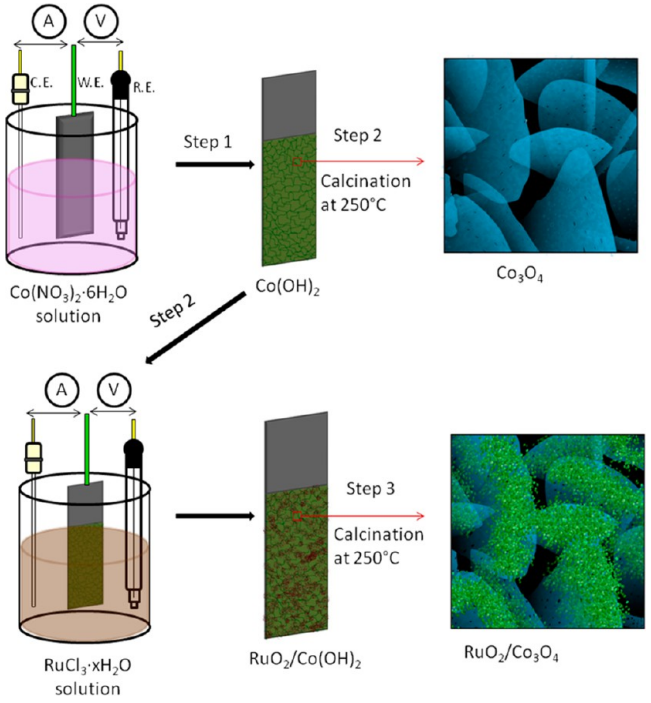

Figure 1. Schematic of the synthesis of Co_3O_4 nanosheet arrays and Co_3O_4/RuO_2 composite films.

In the electrodeposition from an aqueous bath, the following reactions are considered to generate a base at an electrode surface

$$2H_2O + O_2 + 4e^- \Leftrightarrow 4OH^- \tag{6}$$

and

$$2H_2O + 2e^- \Leftrightarrow H_2 + 2OH^- \tag{7}$$

These reactions consume H_2O and generate OH^- ions. The generation of OH^- ions at the cathode raises the local pH value, resulting in the uniform precipitation of $RuO_2{\cdot}xH_2O$ over $Co(OH)_2$ deposit. The final step is the calcination at 250 °C for 2 h for the conversion of $Co(OH)_2$ into mesoporous Co_3O_4 nanosheet array. The film thickness was changed by varying deposition time period as 10, 20, and 30 min respectively.

Field-emission scanning electron microscope (FESEM) image of top view of the intermediate product, $Co(OH)_2$ nanosheet arrays directly deposited over carbon paper substrate is shown in Figure 2 (a). Upon calcination at a ramping rate of 2 °C per min., no significant morphological and structural changes happens to the array, except for the development of mesoporous nature, as evident from the high resolution SEM image of Co_3O_4 nanosheets as shown in images b and c in Figure 2, suggesting good stability of the nanosheet structure. The average thickness of the Co_3O_4 nanosheet can be estimated to be less than 20 nm. The mesoporous nature can be ascribed to the successive release and loss of H_2O during the oxidative transformation of $Co(OH)_2$ to Co_3O_4 during the thermal treatment.[37,38] The morphology of the nanosheet array starts collapsing when the ramping rate is increased above 5 °C per min (Figure 2d).

FESEM image of top view of Co_3O_4 nanosheet arrays obtained by the calcinations of $Co(OH)_2$ nanosheet arrays at a ramping rate of 2 °C per min reveals (Figure 3a) the presence of high density of Co_3O_4 nanosheets perpendicular to the surface of graphitized carbon paper substrate, forming a 3D

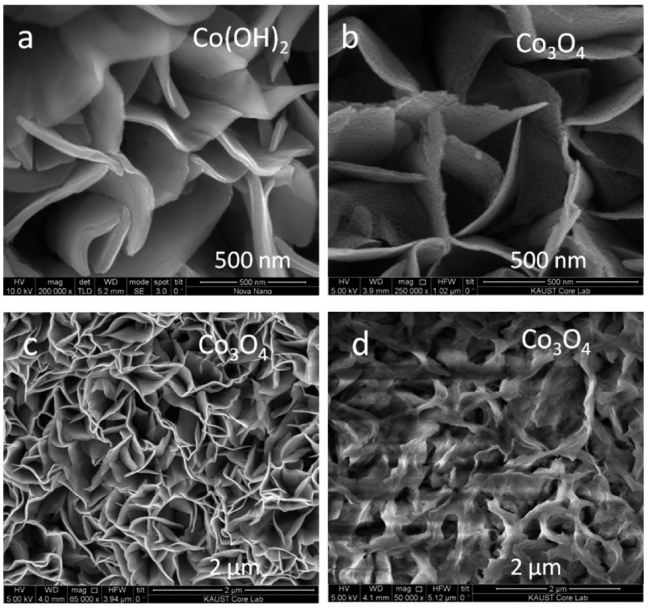

Figure 2. (a) FESEM image of as grown $Co(OH)_2$ nanosheet arrays. (b) High-magnification FESEM image of mesoporous Co_3O_4 nanosheets. (c) FESEM image of Co_3O_4 nanosheet array at a calcination ramping rate of 2 °C per min and (d) FESEM image of collapsed Co_3O_4 nanosheet array when the calcination ramping rate is above 5 °C per min.

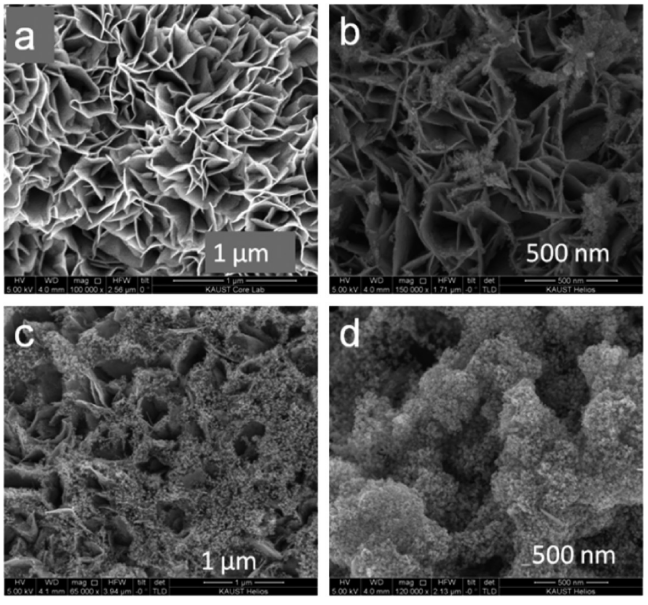

Figure 3. FESEM images of (a) Co_3O_4 nanosheet arrays and Co_3O_4/RuO_2 composite films produced by (b) 10, (c) 20, and (d) 30 min deposition of hydrous RuO_2 nanoparticles.

hierarchical structure with interconnected nanosheets microporous structure. FESEM images of Co_3O_4 /RuO_2 films prepared by, 10, 20, and 30 min of electrodeposition of RuO_2 nanoparticles are shown in Figure 3b–d, respectively. After10 min of RuO_2 deposition, the majority of the area of Co_3O_4 nanosheet array is not coated with RuO_2 nanoparticles. For the sample prepared by 20 min of RuO_2 deposition, the edges of Co_3O_4 nanosheet array are uniformly coated with nanocrystalline RuO_2 particles retaining the open porous structure of the array. After 30 min of RuO_2 deposition, the open mesoporous morphology of the array is completely lost because of the thick layer of the RuO_2 deposit. From the surface morphology it appears that the Co_3O_4 /RuO_2 film prepared by 20 min deposition will be the most suitable one as a supercapacitor electrode as it retains the open structure of the nanosheet array with thicker deposition of conducting RuO_2 nanoparticles at the edges of the sheets. Energy dispersive X-ray analysis (EDAX) pattern and elemental mapping of Co_3O_4 /RuO_2 film prepared by 20 min of RuO_2 deposition are shown in Figure S1a–d in the Supporting Information. The pattern shows the presence of the elements Co, O and Ru. Elemental mapping images show homogeneous dispersion of these elements throughout the surface of the film.

Powder X-ray diffraction (PXRD) patterns of the as-prepared and calcined films on the graphitized carbon paper substrate are shown in Figure 4. In these profiles, the diffraction peaks at 2θ

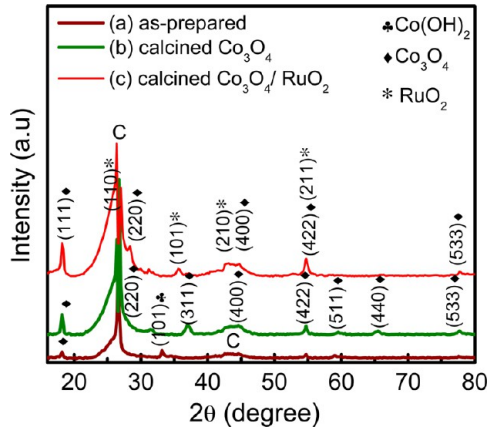

Figure 4. Powder XRD patterns of (a) $Co(OH)_2$ nanosheet arrays (b) Co_3O_4 nanosheet arrays and (c) Co_3O_4/RuO_2 composite films over graphitized carbon paper substrate.

= 26.5 and 43.0° are attributed to graphitic carbon from the substrate. The as-prepared sample obtained (Figure 3a) after the electrodeposition of $Co(OH)_2$ shows a peak corresponding to the reflection from (101) plane of β-$Co(OH)_2$ (JCPDS card no. 30-0443). For the calcined sample (Figure 3b), except for the peaks originating from the substrate, all the diffraction peaks can be indexed to a pure face-centered cubic phase of Co_3O_4 (space group: $Fd3m$ (227), JCPDS card no. 43-1003). No prominent peaks from β-$Co(OH)_2$ can be seen in the pattern. XRD pattern of Co_3O_4 /RuO_2 sample shows reflections from different planes of both tetragonal RuO_2 ((JCPDS 40-1290, 43-1027) and from Co_3O_4. It can also be seen that (110) peak from RuO_2 is overlapping with (002) peak of graphitic carbon.

Figure 5a shows the high-resolution Co 2p spectrum of the sample obtained by calcination of $Co(OH)_2$ nanosheet array. Spectrum consists of two main broad peaks at 794.9 and 779.8 eV corresponding to $2p_{1/2}$, $2p_{3/2}$ spin orbit lines respectively. The spectrum also contains weak satellite structures at the high binding energy side of 2 $p_{1/2}$ and $2p_{3/2}$ main peaks, which indicates the existence of Co in oxide form.[39,40] To identify the oxidation state of Co, we conducted peak fitting of Co $2p_{3/2}$ (Figure 5b). The approach used for the peak fitting is similar to the one used by Biesinger et al.,[41] i.e., fitting of a broad main peak combined with the satellite structure. A shirly background is applied across the Co $2p_{3/2}$ peak of the spectrum. The details are given in the Supporting Information. The Co $2p_{3/2}$ from the

dx.doi.org/10.1021/am405849n | ACS Appl. Mater. Interfaces 2014, 6, 4196–4206

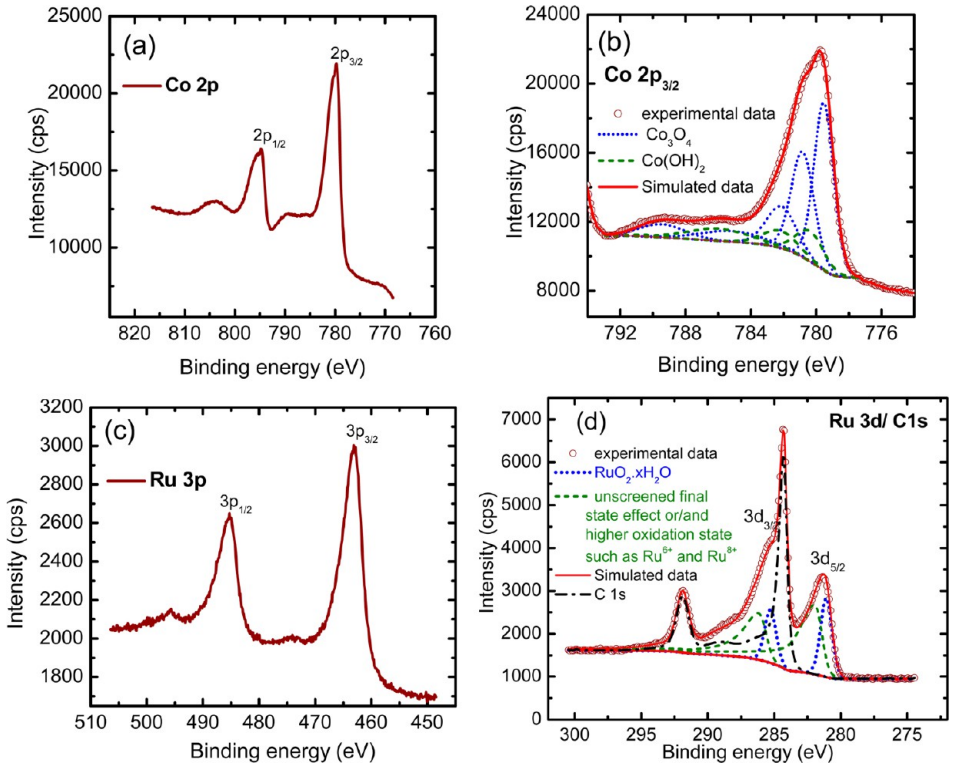

Figure 5. (a) High-resolution Co 2p spectrum, (b) peak fitted high-resolution Co $2p_{3/2}$ peak, (c) high-resolution Ru 3p spectrum, and (d) peak fitted high-resolution Ru 3d spectrum originating from Co_3O_4/RuO_2 composite films over graphitized carbon paper substrate.

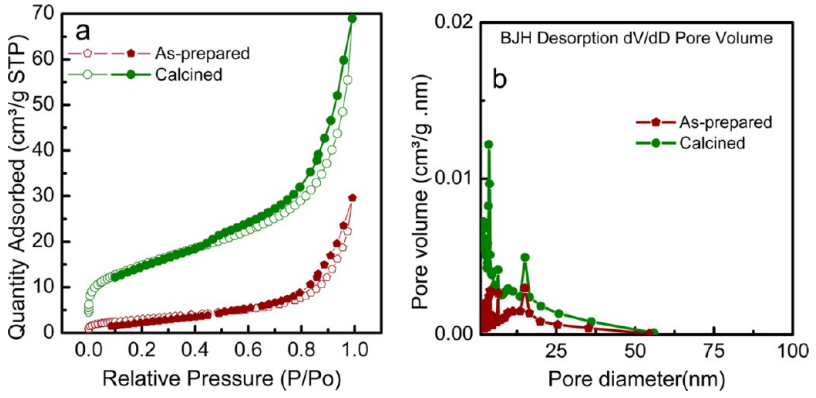

Figure 6. (a) Nitrogen adsorption and desorption isotherms and (b) pore size distribution of the as-prepared $Co(OH)_2$ and calcined Co_3O_4 samples.

calcined sample in Figure 5b is well-fitted using a combination of the parameters derived from both Co_3O_4 and $Co(OH)_2$ standard samples.[41] This indicates that the surface layers of the sample contains small amount of $Co(OH)_2$. XPS is a surface characterization technique, which can give the atomic composition of approximately the upper 5 nm of a sample surface. In the present study the sample thickness is more than 20 micrometers. Hence PXRD results give more detailed idea about the composition of the bulk sample. Absence of $Co(OH)_2$ peak in the PXRD pattern of calcined Co_3O_4 sample clearly eliminates the possibility of having any significant amount of $Co(OH)_2$ in the bulk sample.

Figure S2a in the Supporting Information shows the XPS survey spectrum of the graphitized substrate. FigureS2b in the Supporting Information shows the high-resolution C1s peak arising from the substrate. XPS survey spectrum of RuO_2/Co_3O_4 sample obtained by 20 min electrodeposition of RuO_2 is shown in FigureS2c in the Supporting Information. In addition to the peaks arising from the substrate, the spectrum exhibits peaks corresponding to photoelectron core levels and Auger lines originating from Co and Ru.

Figure 5c shows the high-resolution Ru 3p spectrum of the Co_3O_4/RuO_2 sample obtained by 20 min electrodeposition of RuO_2. Spectrum consists of two main peaks at 485.3 and 463.2 eV corresponding to $3p_{1/2}$, $3p_{3/2}$ spin orbit lines respectively, separated by about 22.1 eV.[42−44] Detailed analysis of Ru 3d spectrum done by peak fitting (Figure 5d) is used to identify the nature of RuO_2 (hydrous/anhydrous) present in the sample. The analysis of high-resolution Ru 3d spectrum is complex due to the overlap of Ru 3d peak with the C 1s peak (285.1 eV) arising from the underlying graphitized carbon support. In order to extract the fitted curve of the C 1s from the

dx.doi.org/10.1021/am405849n | ACS Appl. Mater. Interfaces 2014, 6, 4196−4206

substrate was subtracted from the Ru spectrum. The Ru $3d_{5/2}$ peak occurs at 281.3 eV. For metallic Ru, it has been reported that the Ru 3d5/2 occurs at 280.1 eV, while upon subsequent oxidation, a movement towards higher binding energy is observed and for pristine RuO_2 films, the Ru 3d5/2 peak is reported to be at 281 eV.[42−44] Any small shift in this value towards higher binding energy can be attributed to the presence of hydrous RuO_2 in the sample. Detailed analysis the Ru 3d spectrum upon peak fitting shows two peaks at 285.3 and 281.3 eV corresponding to $3d_{3/2}$, $3d_{5/2}$ spin orbit lines arising from hydrous RuO_2.[42,44] The spectrum also contains two peaks at 286.3 and 282.1 eV which can be attributed to the unscreened final state effect in photoemission or (and) the presence of higher oxidation states such as Ru^{6+} or Ru^{8+}.[42]

The nitrogen adsorption and desorption isotherms of the as-prepared $Co(OH)_2$ and calcined Co_3O_4 samples are shown in Figure 6a. The Brunauer−Emmett−Teller (BET) surface area values calculated for the as-prepared and the calcined samples are respectively 11.2, and 53.1 m^2/g. The calcined sample exhibits a distinct hysteresis loop in the range of 0.45−1.0 P/P_0, which suggests the presence of a mesoporous structure with the maximum BET surface area. This loop is not prominent in the case of the as-prepared sample (in the range of 0.45−1.0 P/P_0). BET surface area value obtained for the calcined sample is higher than the values reported for Co_3O_4 nanoflakes by Xiong et al.[17] and, which is favorable for better supercapacitor performance of the composites. From DFT pore size calculations, the total pore volume values obtained for the as-prepared and calcined samples are respectively 0.03351, and 0.04639 cm^3/g. The pore size distributions of the as-prepared $Co(OH)_2$ and calcined Co_3O_4 samples calculated by desorption isotherms using Barret−Joyner−Halenda (BJH) method are shown in Figure 6(b). BJH Desorption cumulative volume of pores between 1.700 and 300.000 nm diameter for the as-prepared and the calcined samples are respectively 0.046, and 0.104 cm^3/g, respectively.

Detailed information of the inside structure of Co_3O_4 nanosheets were obtained from high-resolution transmission electron microscopy (HRTEM) images in Figure 7a−c. The calcined nanosheets are composed of interconnected crystalline Co_3O_4 nanoparticles with average particle size in the range of 10-15 nm. The nanosheets are porous because of the removal of water molecules at high temperature.[22] The porous nature of the nanosheets as evident from these images will help in increasing the surface area of Co_3O_4, and expected to enhance electrochemical activities. SAED pattern of the Co_3O_4 nanosheet is shown in Figure 7d, which reveals that the nanosheets have a polycrystalline structure. The diffraction rings can be indexed to the cubic Co_3O_4 crystal structure.

Further insight into the morphology and microstructure of the Co_3O_4 and RuO_2/Co_3O_4 nanosheets were obtained by TEM and scanning tunneling microscopy (STM) images shown in Figure 8. The TEM image of Co_3O_4 nanosheet (Figure 8a) shows a porous foam-like inside architecture. A large amount of well-distributed pores (the white points on the surface) can be clearly seen, which is well-consistent with the results observed from SEM. TEM and STM images of RuO_2/Co_3O_4 nanosheets (Figure 8b, c, respectively) show nanocrystalline RuO_2 particles over Co_3O_4 nanosheets. High-resolution TEM (HRTEM) image of crystalline RuO_2 nanoparticles is shown in Figure 8d. The selected-area electron diffraction of RuO_2 nanoparticles (SAED, inset of Figure 8d) could be indexed as a polycrystalline pattern.

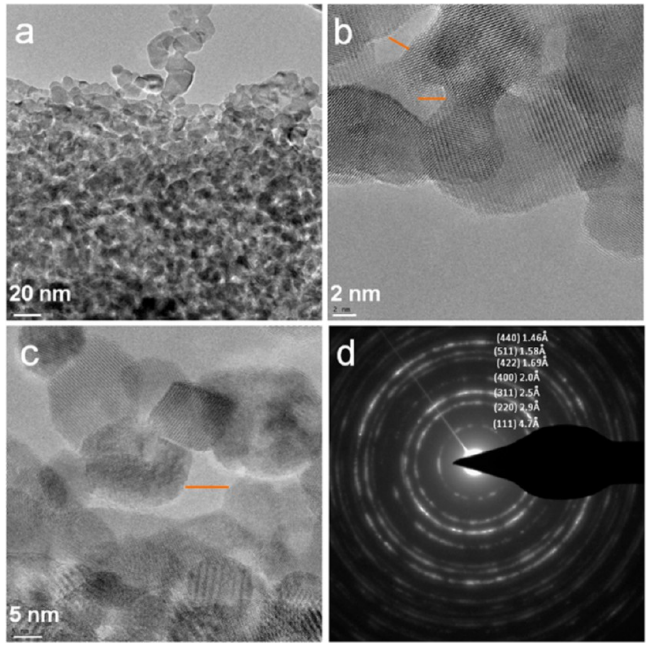

Figure 7. (a−c) HRTEM images of Co_3O_4 nanosheet arrays and (d) SAED pattern of Co_3O_4 nanoparticles.

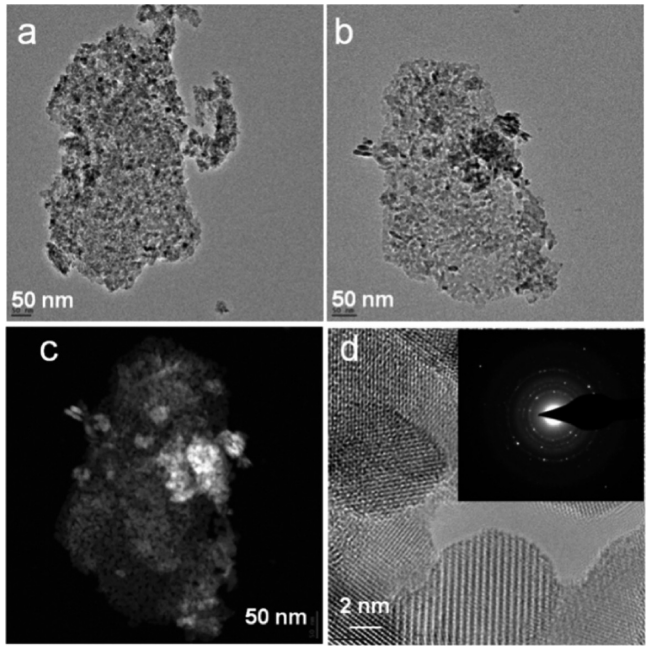

Figure 8. TEM images of (a) Co_3O_4 nanosheet arrays and (b) Co_3O_4/RuO_2 composite films. (c) STM image of Co_3O_4/RuO_2 composite films and (d) HRTEM image of nanocrystalline hydrous RuO_2 nanoparticles (Inset shows the SAED pattern of RuO_2 nanoparticles).

To identify the best-suited electrode material for high-rate capacitive energy storage, symmetric supercapacitors are fabricated using the 4 different samples and cyclic voltammetry (CV) and galvanostatic charge−discharge (CD) measurements are conducted in classical two electrode configurations. It has been reported that as compared to three electrode configuration, measurements using two electrode configuration is more suited for evaluating the performance of a supercapacitor test cell as it mimics the physical configuration, internal voltages, and charge transfer that occurs in a real supercapacitor

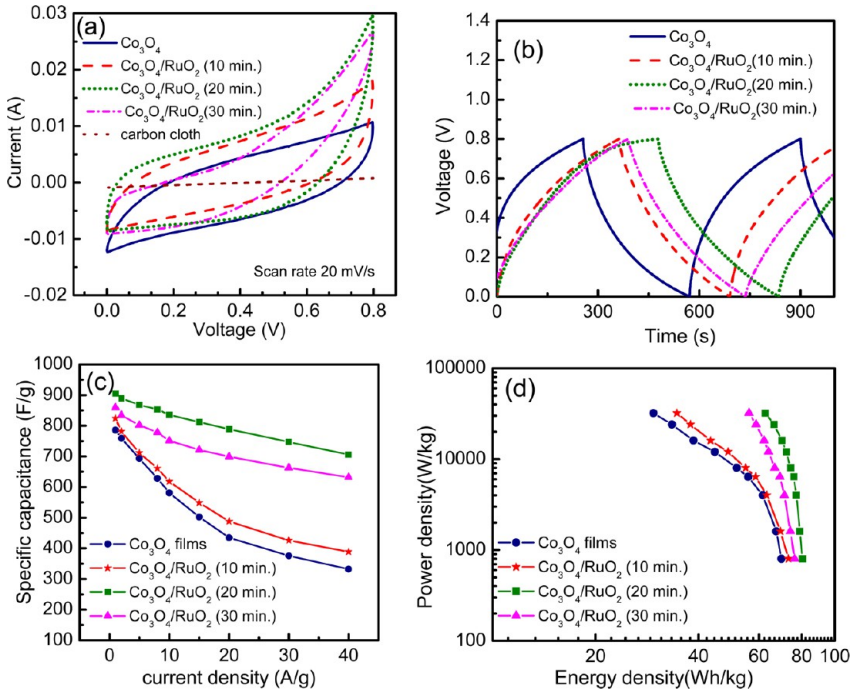

Figure 9. (a) CV loops of symmetric supercapacitors based on the different samples and carbon cloth substrate at a scan rate of 20 mV/s and (b) galvanostatic charge/discharge curves at a constant current density of 1A/g. (c) Variation in specific capacitance values as a function of current density (rate performance) and (d) Ragone plot of symmetric supercapacitors based on the different samples.

application and thus provides the best indication of an electrode material's performance.[27]

A comparison of CV loops of symmetric supercapacitors based on the different samples and carbon cloth substrate at a scan rate of 20 mV/s is shown in Figure 9a. For the same mass loading, the CV curves show different areas indicating different levels of stored charge. It is also evident that the capacitive contribution from the carbon cloth substrate to the electrodes is negligibly small. Because both Co_3O_4 and RuO_2 are excellent pseudocapacitive materials, there is significant pseudocapacitance contribution from each of these metal oxides to the overall measured capacitance.

The mechanism of electrochemical reaction occurring at the Co_3O_4 electrode during the redox process in the CV measurement can be expressed according to eq 8

$$Co_3O_4 + H_2O + OH^- \Leftrightarrow 3CoOOH + e^- \quad (8)$$

From the CV loops specific capacitances of 585, 627, 842, and 762 F/g, respectively (using eq 6) are obtained for the symmetric capacitors based on pure Co_3O_4 and Co_3O_4 /RuO_2 samples with 10, 20, and 30 min deposition of RuO_2. Enhancement in the capacitance values of Co_3O_4/RuO_2 electrodes likely arises from a pseudocapacitance contribution from hydrous RuO_2 through a strong Faradic reaction, which can be expressed using eq 9

$$RuO_2 + \delta H^+ + \delta e^- \Leftrightarrow RuO_{2-\delta}(OH)\delta \ (1 \geq \delta \geq 0) \quad (9)$$

The resultant cyclic voltammograms shown in Figure 9a are having the combined characteristics of double layer capacitance (by virtue of the electrode morphology providing maximum electrolyte accessibility) and Faradaic pseudocapacitance. Absence of peaks in the cyclic voltammogram merely indicates that the electrodes are charged and discharged at a pseudo-constant rate over the complete voltammetric cycle. Figure 9b shows the comparison of galvanostatic charge/discharge curves for the samples at a constant current density of 1 A/g. The constant current charge discharge curves all the devices are nearly triangular, with reduced internal resistance at the beginning of the discharge curve. The reduction in internal resistance may be attributable to the direct contact of active materials and the conducting carbon paper substrate. The specific capacitance values for the supercapacitors based on pure Co_3O_4 and Co_3O_4/RuO_2 samples with 10, 20, and 30 min deposition of RuO_2 respectively are 786, 824, 905, and 859 F/g (using eq 7). These values are much higher than those reported for RuO_2/Co_3O_4 thin films (353 F/g) prepared by spray pyrolysis technique by Li et al.[16] Galvanostatic charge-discharge measurements for the four different symmetric capacitors are carried out at different current current densities (see Figure S3 in the Supporting Information) from 1 A/g to 40 A/g and specific capacitance values are calculated from each of these measurements. High performance supercapacitor electrodes should have high rate performance. Variations in specific capacitances of symmetric supercapacitors based on the different samples with increase in current density are shown in Figure 9c. In general, the specific capacitance decreases with the increase in discharge current density. At lower current densities, ions can penetrate into the inner-structure of electrode material, having access to almost all available pores of the electrode, but at higher current densities, an effective utilization of the material is limited only to the outer surface of electrodes. It results in the reduction of specific capacitance values. Supercapacitors based on Co_3O_4 /RuO_2 composites exhibit superior capacitive performance than the one based on pure Co_3O_4 sample. The symmetric supercapacitor based on Co_3O_4/RuO_2 sample prepared by 20 min electrodeposition of RuO_2 presented the highest specific capacitance value at various current densities. The excellent microstructure and surface morphology of the electrode with uniform distribution of

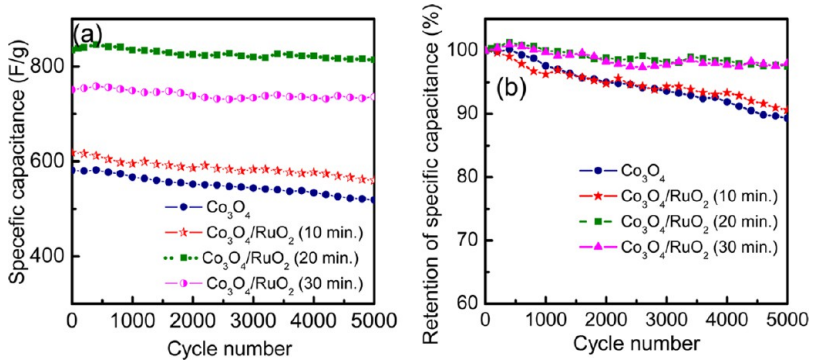

Figure 10. (a) cycling stability performance and (b) % of specific capacitance retention of symmetric supercapacitors based on the different samples.

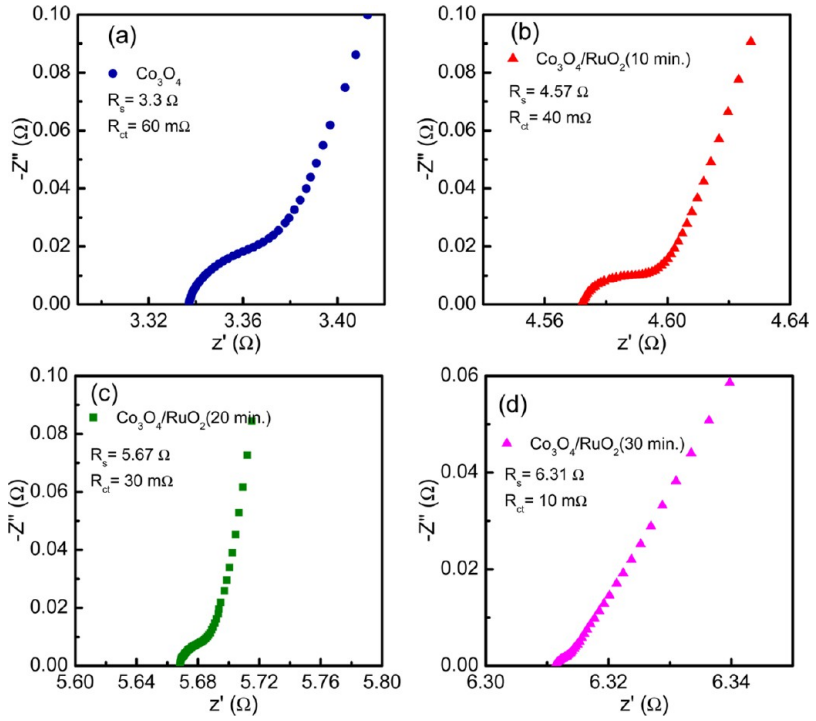

Figure 11. Nyquist plots for pure (a) Co_3O_4 and Co_3O_4/RuO_2 composite electrodes prepared by (b) 10, (c) 20, and (d) 30 min deposition of RuO_2 in a three-electrode configuration.

nanocrystalline RuO_2 over mesoporous Co_3O_4 nanosheet array presents maximum electrolyte accessible surface area for this sample. The specific capacitance retention ratio as a function of the current density can be obtained from Figure 9c. The highest rate capacity (78%) is obtained at the current density ranging from 1 to 40 A/g for the symmetric supercapacitor based on Co_3O_4/RuO_2 composite obtained by 20 min depositon of RuO_2. Rate capacities of 42, 47, and 74%, respectively, are obtained for the symmetric capacitors based on pure Co_3O_4 and Co_3O_4/RuO_2 samples with 10 and 30 min deposition of RuO_2. These results indicate that 20 min. RuO_2 deposition composite suits to high-rate charge/discharge, as it has a lower electron hopping resistance which results in a lower iR at a high-rate charge−discharge. Ragone plot (power density vs. energy density) of the symmetric supercapacitors based on pure Co_3O_4 and Co_3O_4/RuO_2 samples with 10, 20, and 30 min deposition of RuO_2 are shown in Figure 9d. The energy (E) and power densities (P) for the supercapacitors were calculated from charge−discharge curves at different current densities using eq 10 and 11, respectively.

$$E = \frac{1}{2} C_{sp} \Delta V^2 \tag{10}$$

where ΔV is the potential window of discharge process.

$$P = \frac{E}{\Delta t} \tag{11}$$

At a constant power density of 32 kW/kg, the energy densities obtained for supercapacitors based on pure Co_3O_4 and Co_3O_4/RuO_2 samples with 10, 20, and 30 min deposition of RuO_2 are 29, 34, 62 and 56Wh/kg respectively. At a low power density of 0.8 kW/kg, the energy densities reach as high as 69, 73, 80, and 76 Wh/kg respectively. From the analysis of Ragone plot, it is evident that mesoporous Co_3O_4/RuO_2 sample prepared by 20 min deposition of RuO_2 works as a very promising electrode material for high-performance supercapacitors. This sample maintains high power density without much reduction in energy density.

The cycle life is another important factor for evaluating the performance of supercapacitor. Cyclic stability curves and % of

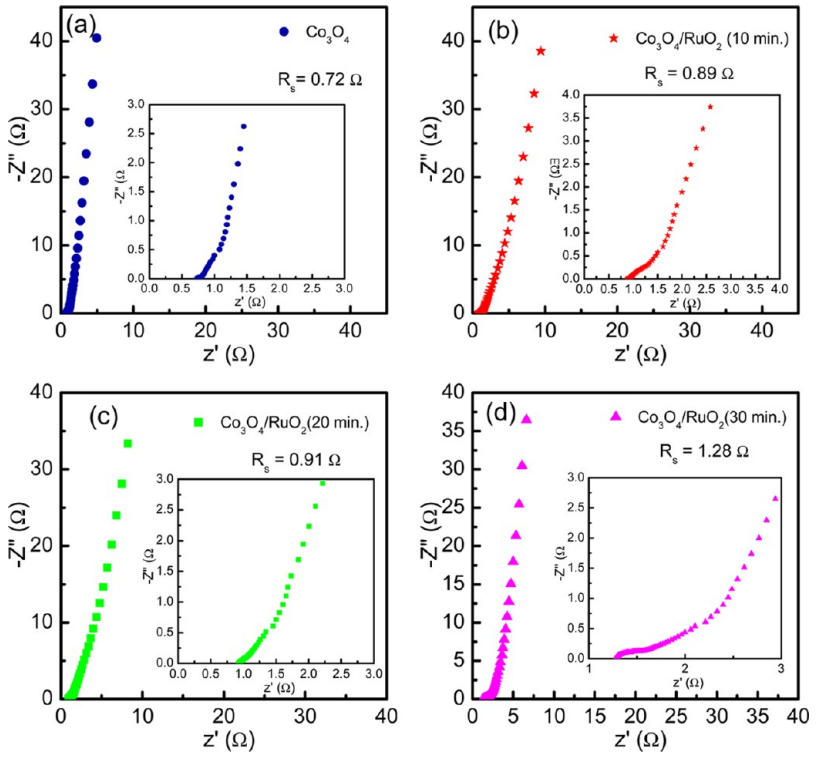

Figure 12. Nyquist plots for (a) pure Co_3O_4 and Co_3O_4/RuO_2 composites prepared by (b) 10, (c) 20, and (d) 30 min deposition of RuO_2-based symmetric capacitors in a classical two-electrode configuration.

specific capacitance retention for symmetric supercapacitors at a constant current density of 10 A/g are illustrated in panels a and b Figure 10, respectively. For Co_3O_4/RuO_2 samples with 20 and 30 min deposition of RuO_2, the specific capacitance increases gradually at the beginning of cycles, and then there is a slight decrease. This phenomenon indicates that there is an initial activation process for Faradaic pseudo-capacitance of electrode materials. During the first 500 cycles, the specific capacitance of sample with 20 min deposition of RuO_2 increases from 835 to 846 F/g and that of Sample with 30 min deposition of RuO_2 increases from 751 to 758 F/g. In the case of supercapacitors based on other two samples, the specific capacitance slowly decreases with increase in cycle numbers. At the end of 5000 cycles, symmetric supercapacitors based on pure Co_3O_4 and Co_3O_4/RuO_2 samples with 10, 20, and 30 min deposition of RuO_2 retain respectively 89, 91, 96, and 97% of their maximum capacitance.

Electrochemical impedance spectroscopy (EIS) measurements can be applied to investigate electrical conductivity and ion transfer properties of the different electrode materials. Figure 11a–d respectively presents the Nyquist impedance plots measured in standard 3 electrode configuration in the frequency range from 100 kHz to 10 mHz at open circuit voltage by applying a 5 mV signal for pure Co_3O_4 and Co_3O_4/RuO_2 composites prepared by 10, 20, and 30 min deposition of RuO_2. The impedance spectra can be divided into two regions by the so-called knee frequency, with a semicircle arc in the high frequency region and a straight line in the low frequency region. In the high frequency range, the intercept at real part (Z') is a combinational resistance of ionic resistance of electrolyte, intrinsic resistance of substrate, and contact resistance between the active material and the current collector. These values for pure Co_3O_4 and Co_3O_4/RuO_2 composites prepared by 10, 20, and 30 min deposition of RuO_2 electrodes are 3.3, 4.6, 5.7, and 6.3 Ω, respectively. A comparison of the Nyquist plots of the samples are shown in Figure S4a in the Supporting Information. Since the values of ionic resistance of electrolyte (R_s) and intrinsic resistance of substrate are the same for all the samples, the different values imply the difference of the contact resistance between the active material and the current collector. The contact resistance of different Co_3O_4/RuO_2 composites increases gradually with the increase of RuO_2 content. The semicircle arc observed in the high frequency region results from a parallel combination of the charge-transfer resistance (R_{ct}) caused by faradaic reactions and the double-layer capacitance (C_{DL}). The charge-transfer resistance (R_{ct}) from the diameter of the semicircle for pure Co_3O_4 and Co_3O_4/RuO_2 composites prepared by 10, 20, and 30 min deposition of RuO_2 electrodes are calculated as 0.06, 0.04, 0.03and 0.01 Ω, respectively. The charge-transfer resistance (R_{ct}) decreases gradually with the increase of RuO_2 content, which indicates the improvement in the conductivity of the composite films.

Figure 12a–d respectively shows the experimental Nyquist impedance spectra for symmetric supercapacitor test cells based on pure Co_3O_4 and Co_3O_4 /RuO_2 composites prepared by 10, 20, and 30 min deposition of RuO_2. In the present study all the samples exhibit very low value for R_{ct}, indicating high conductivity of the electrodes with excellent electrolyte accessibility. The line at the low-frequency region making an angle 45° with the real axis is the Warburg line which is a result of the frequency dependence of ion diffusion in the electrolyte to the electrode interface. Experimental results show that the magnitude of ESR obtained from the x-intercept of the Impedance spectra for symmetric supercapacitor test cells based on pure Co_3O_4 and Co_3O_4 /RuO_2 composites prepared by 10, 20, and 30 min deposition of RuO_2 are 0.72, 0.89, 0.91, and 1.02 Ω, respectively. These lower values indicate consistent

dx.doi.org/10.1021/am405849n | ACS Appl. Mater. Interfaces 2014, 6, 4196–4206

interfacial contact between the nanocrystalline RuO_2 dispersed mesoporous Co_3O_4 nanosheet arrays and the carbon substrates. The impedance characteristics are analyzed based on a equivalent circuit,[45] as depicted shown in Figure S4b in the Supporting Information. In the circuit model, C_p represents the pseudocapacitance of the active materials.

Because of their small particle size, high surface to volume ratio, and higher surface energy, nanomaterials inherently exhibit higher electrocatalytic activities as compared to their bulk counterparts. Hydrous RuO_2 deposited over mesoporous Co_3O_4 nanosheet arrays in the present study are crystalline nanoparticles. In the case of the Co_3O_4 /RuO_2 composite prepared by 30 min deposition of RuO_2, a coagulation of nanoparticles occurs due to their high surface energy. This invariably leads to an under-utilization of the active material leading to a loss of material performance. Moreover, the underlying morphology of the Co_3O_4 nanosheet array is lost, leading to a reduction in electrolyte accessible surface area and thus the total capacitance. Thus, it is highly desirable that the nanoparticle is dispersed uniformly with good adherence to the underlying support material. SEM images of Co_3O_4/RuO_2 samples with 30 min and 20 min deposition of RuO_2 after the cycling studies are shown in a and b and c and d, respectively, in Figure S5 in the Supporting Information. The rate performance of supercapacitors can be improved by the enhancement in the kinetics of ion and electron transport in electrodes and at the electrode/electrolyte interface and by exposing more electroactive species for the Faradaic redox reaction. This happens in the case of Co_3O_4 /RuO_2 composite prepared by 20 min deposition of RuO_2, where the underlying morpohology of the nanosheet array is also retained, leading in the improvement in the conductivity specific capacitance and rate capability, thereby making the composite electrode an ideal one for the fabrication of high rate supercapacitor.

4. CONCLUSIONS

In summary, we have demonstrated that the rate performance of mesoporous Co_3O_4 nanosheet arrays grown directly over carbon cloth collectors can be improved by the uniform dispersion of hydrous RuO_2 nanoparticles. The Co_3O_4/RuO_2 nanostructured electrode morphology was tuned by controlling the electrodeposition time to achieve a balance between good electrode conductivity and efficient electrolyte access to the RuO_2 nanoparticles, hence optimizing perfromance. A high specific capacitance value (905 F/g at 1 A/g), high rate performance of 78% at the current density ranging from 1 to 40 A g^{-1}, and excellent cycling stability (96% after 5000 charge discharge cycles) were achieved using symmetric two-electrode configuration.

■ ASSOCIATED CONTENT

Supporting Information

Energy-dispersive X-ray analysis (EDAX) pattern and elemental mapping of RuO_2 /Co_3O_4 film, details of peak fitting of Co 2p3/2 peak from the calcined $Co(OH)_2$ nanosheet array, galvanostatic charge−dischare curves at different current densities for the symmetric capacitors based on pure Co_3O_4 and RuO_2 /Co_3O_4 samples, Nyquist plots for Co_3O_4 and Co_3O_4/RuO_2 composite electrodes in a three-electrode configuration and equivalent circuit, SEM images of Co_3O_4/RuO_2 samples with 30 min and 20 min deposition of RuO_2 after the cycling studies. This material is available free of charge via the Internet at http://pubs.acs.org/.

■ AUTHOR INFORMATION

Corresponding Author

*E-mail: husam.alshareef@kaust.edu.sa. Phone: +966-(0)2-808-4477.

Notes

The authors declare no competing financial interest.

■ ACKNOWLEDGMENTS

Authors thank Advanced nanofabricationNanofabrication, Imaging and Characterization Laboratory and Analytical Chemistry Core Laboratory at KAUST and Olga Zausalina for the graphical illustration design. R.B.R. acknowledges the financial support from SABIC Post-Doctoral Fellowship. W.C. acknowledges support from KAUST Graduate Fellowship. H.N.A. acknowledges the generous support from KAUST Baseline Fund.

■ REFERENCES

(1) Simon, P.; Gogotsi, Y. Materials For Electrochemical Capacitors. *Nat. Mater.* **2008**, *7* (11), 845−854.

(2) Conway, B. E., *Electrochemical Supercapacitors: Scientific Fundamentals and Technological Applications*. Kluwer Academic/Plenum: New York, 1999.

(3) Conte, M. Supercapacitors Technical Requirements for New Applications. *Fuel Cells* **2010**, *10* (5), 806−818.

(4) Naoi, K. "Nanohybrid Capacitor": The Next Generation Electrochemical Capacitors. *Fuel Cells* **2010**, *10* (5), 825−833.

(5) Guerrero, M. A.; Romero, E.; Barrero, F.; Milanes, M. I.; Gonzalez, E. Supercapacitors: Alternative Energy Storage Systems. *Przegl. Elektrotech.* **2009**, *85* (10), 188−195.

(6) Wang, G. P.; Zhang, L.; Zhang, J. J. A Review Of Electrode Materials For Electrochemical Supercapacitors. *Chem. Soc. Rev.* **2012**, *41* (2), 797−828.

(7) Calvo, E. G.; Arenillas, A.; Menendez, J. A.; Gonzalez, M.; Viera, J. C. Properties, Advantages And Disadvantages Of Materials Used In Supercapacitors. *Afinidad* **2009**, *66* (543), 380−387.

(8) Zhang, Y.; Feng, H.; Wu, X. B.; Wang, L. Z.; Zhang, A. Q.; Xia, T. C.; Dong, H. C.; Li, X. F.; Zhang, L. S. Progress Of Electrochemical Capacitor Electrode Materials: A Review. *Int. J. Hydrogen Energy* **2009**, *34* (11), 4889−4899.

(9) Inagaki, M.; Konno, H.; Tanaike, O. Carbon Materials For Electrochemical Capacitors. *J. Power Sources* **2010**, *195* (24), 7880−7903.

(10) Jayalakshmi, M.; Balasubramanian, K. Simple Capacitors to Supercapacitors - An Overview. *Int. J. Electrochem. Sci.* **2008**, *3* (11), 1196−1217.

(11) Jacob, G. M.; Yang, Q. M.; Zhitomirsky, I. Composite Electrodes For Electrochemical Supercapacitors. *J. Appl. Electrochem.* **2009**, *39* (12), 2579−2585.

(12) Deori, K.; Ujjain, S. K.; Sharma, R. K.; Deka, S. Morphology Controlled Synthesis of Nanoporous Co_3O_4 Nanostructures and Their Charge Storage Characteristics in Supercapacitors. *ACS Appl. Mater. Interfaces* **2013**, *5* (21), 10665−10672.

(13) Bi, R. R.; Wu, X. L.; Cao, F. F.; Jiang, L. Y.; Guo, Y. G.; Wan, L. J. Highly Dispersed RuO_2 Nanoparticles on Carbon Nanotubes: Facile Synthesis and Enhanced Supercapacitance Performance. *J. Phys. Chem. C* **2010**, *114* (6), 2448−2451.

(14) Zheng, J. P.; Cygan, P. J.; Jow, T. R. Hydrous Ruthenium Oxide As An Electrode Material For Electrochemical Supercapacitors. *J. Electrochem. Soc.* **1995**, *142* (8), 2699−2703.

(15) Rakhi, R. B.; Chen, W.; Cha, D. K.; Alshareef, H. N. High Performance Supercapacitors Using Metal Oxide Anchored Graphene Nanosheet Electrodes. *J. Mater. Chem.* **2011**, *21* (40), 16197−16204.

(16) Li, Y. H.; Huang, K. L.; Zeng, D. M.; Liu, S. Q.; Yao, Z. F. RuO_2/Co_3O_4 Thin Films Prepared By Spray Pyrolysis Technique For Supercapacitors. *J. Solid State Electrochem.* **2010**, *14* (7), 1205−1211.

(17) Xiong, S. L.; Yuan, C. Z.; Zhang, M. F.; Xi, B. J.; Qian, Y. T. Controllable Synthesis of Mesoporous Co3O4 Nanostructures with Tunable Morphology for Application in Supercapacitors. *Chem.—Eur. J.* **2009**, *15* (21), 5320−5326.
(18) Rakhi, R. B.; Chen, W.; Cha, D. Y.; Alshareef, H. N. Substrate Dependent Self-Organization of Mesoporous Cobalt Oxide Nanowires with Remarkable Pseudocapacitance. *Nano Lett.* **2012**, *12* (5), 2559−2567.
(19) Gan, W. P.; Ma, H. R.; Li, X. Preparation and Performance of $(RuO_2/Co_3O_4)\cdot nH_2O$ Composite Films in Super Capacitor. *J. Inorg. Mater.* **2011**, *26* (8), 823−828.
(20) Liu, Y.; Zhao, W. W.; Zhang, X. G. Soft Template Synthesis Of Mesoporous $Co_3O_4/RuO_2\cdot xH_2O$ Composites For Electrochemical Capacitors. *Electrochim. Acta* **2008**, *53* (8), 3296−3304.
(21) Gao, Y. Y.; Chen, S. L.; Cao, D. X.; Wang, G. L.; Yin, J. L. Electrochemical Capacitance Of Co_3O_4 Nanowire Arrays Supported On Nickel Foam. *J. of Power Sources* **2010**, *195* (6), 1757−1760.
(22) Qing, X. X.; Liu, S. Q.; Huang, K. L.; Lv, K. Z.; Yang, Y. P.; Lu, Z. G.; Fang, D.; Liang, X. X. Facile Synthesis Of Co_3O_4 Nanoflowers Grown On Ni Foam With Superior Electrochemical Performance. *Electrochim. Acta* **2011**, *56* (14), 4985−4991.
(23) Kandalkar, S. G.; Lee, H. M.; Chae, H.; Kim, C. K. Structural, Morphological, And Electrical Characteristics Of The Electrodeposited Cobalt Oxide Electrode For Supercapacitor Applications. *Mater. Res. Bull.* **2011**, *46* (1), 48−51.
(24) Wu, J. B.; Lin, Y.; Xia, X. H.; Xu, J. Y.; Shi, Q. Y. Pseudocapacitive Properties Of Electrodeposited Porous Nanowall Co3O4 Film. *Electrochim. Acta* **2011**, *56* (20), 7163−7170.
(25) Yuan, Y. F.; Xia, X. H.; Wu, J. B.; Huang, X. H.; Pei, Y. B.; Yang, J. L.; Guo, S. Y. Hierarchically Porous Co_3O_4Film With Mesoporous Walls Prepared Via Liquid Crystalline Template For Supercapacitor Application. *Electrochem. Commun.* **2011**, *13* (10), 1123−1126.
(26) Yuan, C. Z.; Yang, L.; Hou, L. R.; Shen, L. F.; Zhang, X. G.; Lou, X. W. Growth Of Ultrathin Mesoporous Co3O4 Nanosheet Arrays On Ni Foam For High-Performance Electrochemical Capacitors. *Energy Environ. Sci.* **2012**, *5* (7), 7883−7887.
(27) Stoller, M. D.; Ruoff, R. S. Best Practice Methods For Determining An Electrode Material's Performance For Ultracapacitors. *Energy Environ. Sci.* **2010**, *3* (9), 1294−1301.
(28) Xing, W.; Qiao, S. Z.; Wu, X. Z.; Gao, X. L.; Zhou, J.; Zhuo, S. P.; Hartono, S. B.; Hulicova-Jurcakova, D. Exaggerated Capacitance Using Electrochemically Active Nickel Foam As Current Collector In Electrochemical Measurement. *J. Power Sources* **2011**, *196* (8), 4123−4127.
(29) Palmas, S.; Ferrara, F.; Vacca, A.; Mascia, M.; Polcaro, A. M. Behavior Of Cobalt Oxide Electrodes During Oxidative Processes In Alkaline Medium. *Electrochim. Acta* **2007**, *53* (2), 400−406.
(30) Wang, H.; Zhang, L.; Tan, X.; Hol, C.M.B.; Zahiri, B.; Olsen, B. C.; Mitlin, D. Supercapacitive Properties of Hydrothermally Synthesized Co_3O_4 Nanostructures. *J. Phys. Chem. C* **2011**, *115*, 17599−17605.
(31) Meher, S. K.; Rao, G. R. Effect of Microwave on the Nanowire Morphology, Optical, Magnetic, and Pseudocapacitance Behavior of Co_3O_4. *J. Phys. Chem. C* **2011**, *115* (51), 25543−25556.
(32) Zhang, L. C. J. L. X. G. Preparation And Properties Of Co_3o_4 Nanorods As Supercapacitor Material. *J. Appl. Electrochem.* **2009**, *39*, 1871−1876.
(33) Fedorov, F. S.; Linnemann, J.; Tschulik, K.; Giebeler, L.; Uhlemann, M.; Gebert, A. Capacitance Performance Of Cobalt Hydroxide-Based Capacitors With Utilization Of Near-Neutral Electrolytes. *Electrochim. Acta* **2013**, *90*, 166−170.
(34) Kung, C.-W.; Chen, H.-W.; Lin, C.-Y.; Vittal, R.; Ho, K.-C. Synthesis Of Co_3O_4 Nanosheets Via Electrodeposition Followed By Ozone Treatment And Their Application To High-Performance Supercapacitors. *J. Power Sources* **2012**, *214* (0), 91−99.
(35) Dinamani, M.; Kamath, P. V. Electrocatalysis Of Oxygen Evolution At Stainless Steel Anodes By Electrosynthesized Cobalt Hydroxide Coatings. *J. Appl. Electrochem.* **2000**, *30* (10), 1157−1161.
(36) Park, B. O.; Lokhande, C. D.; Park, H. S.; Jung, K. D.; Joo, O. S. Cathodic Electrodeposition Of RuO_2 Thin Films From Ru(III)Cl-3 Solution. *Mater. Chem. Phys.* **2004**, *87* (1), 59−66.
(37) Wang, G. X.; Shen, X. P.; Horvat, J.; Wang, B.; Liu, H.; Wexler, D.; Yao, J. Hydrothermal Synthesis and Optical, Magnetic, and Supercapacitance Properties of Nanoporous Cobalt Oxide Nanorods. *J. Phys. Chem. C* **2009**, *113* (11), 4357−4361.
(38) Chen, G.; Fu, E.; Zhou, M.; Xu, Y.; Fei, L.; Deng, S.; Chaitanya, V.; Wang, Y.; Luo, H. A Facile Microwave-Assisted Route To $Co(OH)_2$ And Co_3O_4 Nanosheet For Li-Ion Battery. *J. Alloys Compd.* **2013**, *578* (0), 349−354.
(39) Li, D. B.; Liu, X. H.; Zhang, Q. H.; Wang, Y.; Wan, H. L. Cobalt and Copper Composite Oxides as Efficient Catalysts for Preferential Oxidation of CO in H_2 Rich Stream. *Catal. Lett.* **2009**, *127* (3-4), 377−385.
(40) Younis, A.; Chu, D. W.; Lin, X.; Lee, J.; Li, S., Bipolar Resistive Switching in p-Type Co_3O_4 Nanosheets Prepared By Electrochemical Deposition. *Nanoscale Res. Lett.* **2013**, *8*.
(41) Biesinger, M. C.; Payne, B. P.; Grosvenor, A. P.; Lau, L. W. M.; Gerson, A. R.; Smart, R. S. Resolving Surface Chemical States In XPS Analysis Of First Row Transition Metals, Oxides And Hydroxides: Cr, Mn, Fe, Co and Ni. *Appl. Surf. Sci.* **2011**, *257* (7), 2717−2730.
(42) Soin, N.; Roy, S. S.; Mitra, S. K.; Thundat, T.; McLaughlin, J. A. Nanocrystalline Ruthenium Oxide Dispersed Few Layered Graphene (FLG) Nanoflakes As Supercapacitor Electrodes. *J. Mater. Chem.* **2012**, *22* (30), 14944−14950.
(43) Bianchi, C. L.; Ragaini, V.; Cattania, M. G. An XPS Study On Ruthenium Compounds And Catalysts. *Mater. Chem. Phys.* **1991**, *29* (1-4), 297−306.
(44) Chan, H. Y. H.; Takoudis, C. C.; Weaver, M. J. High-Pressure Oxidation Of Ruthenium As Probed By Surface-Enhanced Raman And X-Ray Photoelectron Spectroscopies. *J. Catal.* **1997**, *172* (2), 336−345.
(45) Rakhi, R. B.; Chen, W.; Cha, D.; Alshareef, H. N. Nanostructured Ternary Electrodes for Energy-Storage Applications. *Adv. Energy Mater.* **2012**, *2* (3), 381−389.